Relation between strain and composition in coherent epitaxial Cu/Ni multilayers: Influence of strong concentration gradients

Jean-Marc Roussel,* Stéphane Labat, and Olivier Thomas
Aix-Marseille Université, IM2NP, CNRS UMR 6242, Case 262, Faculté des Sciences de Saint-Jérôme, F-13397 Marseille Cedex 20, France

(Received 21 October 2008; published 26 January 2009)

According to models based on continuum elasticity, strain in a coherent multilayer has a polynomial dependence with the local composition. By performing atomistic calculations within a tight-binding potential, we show that composition gradients also affect the coherency strain in Cu-Ni multilayers having a modulation length in the nanometer range. This additional dependence is due to the presence of interfacial relaxation in these metallic systems. A Fourier analysis of the strain resulting from (100) sinusoidal composition multilayers allows us to identify the main missing terms in the continuum models that account for these composition gradient effects. Beyond this fundamental finding, we discuss how the derived extended model should be useful to extract both composition and strain fields from an x-ray scattering experiment on such multilayers.

DOI: 10.1103/PhysRevB.79.014111 PACS number(s): 62.25.−g, 68.65.Ac, 61.05.cp

I. INTRODUCTION

Recently, kinetic Monte Carlo simulations have revealed a wealth of behaviors concerning the interdiffusion modes in annealed Cu/Ni multilayers. Interdiffusion is expected to proceed by a layer-by-layer mode even though the Cu/Ni system is completely miscible at high temperature. This particular kinetics is controlled by the strong asymmetry of the atomic mobilities in this system that also might be responsible for transient sharpening of the interfaces.[1] In this work, we wonder how such phenomena may be evidenced by performing x-ray scattering experiments. In principle, this nondestructive method provides the pertinent quantities (angular shift, peak intensities) which are sensitive to interdiffusion.[2] However, a full analysis of the x-ray diffractograms giving access to both the lattice strain and the chemical composition requires a realistic model that links these two fields together.

In this context, the aim of this study is to investigate the relation between strain and composition in multilayered Cu/Ni deposit by comparing atomistic calculations (with semi-empirical *N*-body potentials) to the classical Cahn's formulation of coherency strain in chemical inhomogeneous solid solutions.[3] Cahn's continuum model relies on the elasticity theory and was originally restricted to composition wavelengths that are large with respect to the interatomic distance. In this work, we show for the CuNi system that indeed the continuum approach fails in predicting interplane distances in regions having strong concentration gradients (i.e., for wavelengths roughly below 20 interplane distances). However, by Fourier analyzing the strain fields obtained in our simulations, we show that a simple extension of Cahn's continuum model with additional concentration gradient terms enables to recover an analytical predictive model for both long and short composition wavelengths. Interestingly, some prospective calculations of x-ray diffractograms indicate that x-ray scattering experiments should be capable to evidence these concentration gradient effects on the lattice strain.

The paper is organized as follows. In Sec. II, we briefly present the tight-binding (TB) second-moment approximation potential (SMA) derived in the past for transition-metal alloys.[4,5] The SMA parameters are then adjusted to reproduce the main chemical and elastic properties in the CuNi solid solution. A test of the SMA potential is also provided from the calculation of strain in epitaxial Ni-films grown on Cu(100) for which both calculations and measurements are available.[6–8] Then in Sec. III A, we treat the case of a coherent epitaxial multilayer having (001) sharp interfaces. In Sec. III B, we extend our study to CuNi coherent multilayers having diffuse interfaces with sinusoidal concentration profiles. In Sec. III C, we propose a simple extension of the continuum models to describe the strain/composition relation in presence of strong concentration gradient. We then examine in Sec. IV how these composition gradient effects could be evidenced from future x-ray scattering experiments. Finally in Sec. V, a summary of our results is given.

II. MODEL

A. SMA potential

The atomic interactions in CuNi multilayers are described within the SMA potential derived in the past from the tight-binding formalism.[4,9] This analytical potential was quite successful in predicting structural properties in pure fcc metals and alloys.[10] The *N*-body character of the SMA potential gives for instance realistic vacancy formation energies, proper surface relaxations, and good elastic anisotropy when interactions are extended up to the second-neighbor atom distances.

According to the SMA potential, the energy E_n^i of an atom of type $i=A$ or B on the site n having neighbor atoms of type $j=A$ or B on the sites m at distances r_{nm}, writes

$$E_n^i = -\sqrt{\sum_m \beta_{ij}^2 \exp\left[-2q_{ij}\left(\frac{r_{nm}}{r_0^{ij}}-1\right)\right]} + \sum_m A_{ij}\exp\left[-p_{ij}\left(\frac{r_{nm}}{r_0^{ij}}-1\right)\right], \quad (1a)$$

where A_{ij}, β_{ij}, p_{ij}, and q_{ij} are the 12 parameters to be ad-

TABLE I. Values of the SMA parameters used in this work.

(i,j)	A_{ij}	p_{ij}	q_{ij}	β_{ij}	r_0^{ij} (Å)
(Cu,Cu)	0.1084	10.377	2.6335	1.3434	2.56
(Ni,Ni)	0.1217	10.763	2.4349	1.6396	2.49
(Cu,Ni)	0.1529	9.6999	2.9569	1.6281	2.525

justed. r_0^{ii} is the first neighbor distance in the pure fcc metal structure of type i, and r_0^{ij} is arbitrary fixed to the average value $(r_0^{ii}+r_0^{jj})/2$. To perform molecular statics (MS) simulations within this type of semiempirical potentials, cutoff functions in Eq. (1) are generally introduced to avoid any discontinuities in energies and forces. In this work, we use the cutoff function proposed by Creuze *et al.* (see Ref. 11 for more details). This latter consists in replacing the exponential terms in Eq. (1) by fifth-order polynomial forms for interactions distances r_{nm} greater than the next-nearest-neighbor distances. Note also that the cutoff distances at which the interactions vanish are the fourth-nearest-neighbor distances in order to give the proper relative stability between fcc and bcc structures.[11]

In Table I, we report the values of the parameters A_{ij}, β_{ij}, p_{ij}, and q_{ij} used in this work. For pure metals, the fitting procedure[11] consists in reproducing the experimental values of the cohesive energies, the atomic volumes, the bulk moduli, and the Rose universal equation.[12] Concerning now the Cu-Ni interactions, the four crossed parameters are adjusted from the following experimental data: the alloy heats of solution for single substitutional impurities $[E_{\mathrm{sol}}^{\mathrm{Cu\ in\ Ni}} \approx 0.11$ eV and $E_{\mathrm{sol}}^{\mathrm{Ni\ in\ Cu}} \approx 0.03$ eV (Ref. 13)], the bulk modulus $B \approx (B^{\mathrm{Cu}}+B^{\mathrm{Ni}})/2$ (Ref. 14) and the lattice parameter $a_0 \approx (a_0^{\mathrm{Cu}}+a_0^{\mathrm{Ni}})/2$ (Refs. 15–17) of a $Cu_{0.5}Ni_{0.5}$ solid solution. Note that these four quantities depend on lattice relaxation effects and have required molecular statics calculations in this work.

B. Bulk properties

For sake of clarity, we only present here the bulk properties resulting from the SMA potential (and its parameters obtained in Sec. II A) that are pertinent thereafter in this study. We first determine the Ni concentration dependence of the average lattice parameter $a_0(c)$ of an ideal solid solution $Cu_{1-c}Ni_c$. This was achieved by placing randomly the Ni and Cu atoms on a fcc structure of lattice parameter a, in a simulation box having periodic conditions in the three directions. Then, MS calculations give access to the fully relaxed positions of the atoms in the structure and the corresponding energy at $T=0$ K. By repeating these calculations from various a values, one obtains the average lattice parameter $a_0(c)$ that minimizes the energy of $Cu_{1-c}Ni_c$ system at a given Ni concentration c. As a result of these calculations, we find that the c dependence of $a_0(c)$ can be well described by the following expansion:

$$a_0(c) \approx a_0(c_0)[1 + \eta_1(c-c_0) + \eta_2(c-c_0)^2 + \eta_3(c-c_0)^3], \tag{2}$$

with $c_0=0.5$, $a_0(0.5)=3.57194$ Å, $\eta_1=-26.7\ 10^{-3}$, $\eta_2=-1.14\ 10^{-3}$, and $\eta_3=-3.90\ 10^{-3}$. Equation (2) corresponds to an almost linear behavior $(\eta_1 \gg \eta_2, \eta_3)$ that is consistent with Vegard's law observed experimentally in this system.[15–17]

According to elasticity theory, the ratio between the two second-order elastic constants C_{12} and C_{11} controls the perpendicular strain field in a coherent epitaxial CuNi multilayer having a free [100] surface. It is therefore of interest to know how these quantities vary with the concentration c in an homogeneous alloy. To determine $C_{11}(c)$ and $C_{12}(c)$, we perform systematic MS calculations of deformed simulation boxes with respect to the average $a_0(c)$ value obtained previously. The results of these calculations are plotted in Fig. 1 and compared to experimental data. For pure Cu $(c=0)$ and pure Ni $(c=1)$ crystals, we also calculate the third-order elastic constants C_{111}, C_{112}, and C_{123} that might also play a role in the tetragonal deformation considered in this work. In practice, the strain tensors described in Refs. 18 and 19 were applied for these calculations. In Table II, values of these elastic constants are reported and compared to experimental data.[20,21]

Considering the simple form of the SMA potential, the resulting elastic properties shown in Fig. 1 and in Table II are in quite good agreement with experimental data. The main discrepancy appears for the Ni value of C_{11} that is underestimated. On the other hand the energy variation under hydrostatic deformation that are related to the bulk modulus $B=(C_{11}+2C_{12})/3$ and to the anharmonicity of the SMA poten-

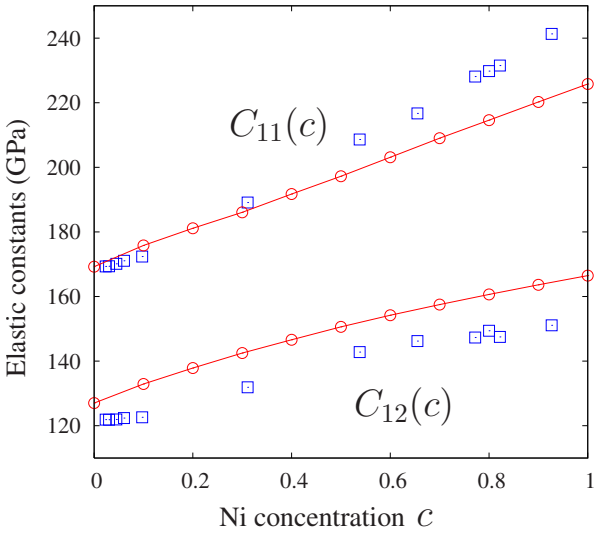

FIG. 1. (Color online) Elastic constants $C_{11}(c)$ and $C_{12}(c)$ as a function of the Ni concentration c in an ideal CuNi solid solution: (○) calculated values from the SMA potential; (□) experimental data (Ref. 14).

TABLE II. Some elastic constants (in GPa) of the pure elements according to the SMA potential and compared to experimental values

	B	C_{11}	C_{12}	C_{111}	C_{112}	C_{123}
Cu	141	169	127	−1430	−950	−170
Ref. 20	135	166	120	−1271	−814	−50
Ni	186	225	166	−1970	−1310	−210
Ref. 21	184	250	151	−2100	−1340	60

tial [through the combination of the constants B and $C_{111}+6C_{112}+2C_{123}$ (Refs. 18 and 19)] are correctly reproduced. This is also the case for the $B(c)$ variation that increases almost linearly as expected from experiments.

Anticipating again the comparison between continuum and atomistic approaches made in this work, it is also instructive to discuss how the ratio $2C_{12}/C_{11}$ varies with the concentration c. From Fig. 1, this latter is found to be almost constant with c (close to the value of 1.5) while a decrease with c is observed experimentally (from 1.45 to 1.21). This limitation of our interatomic potential is due to the underestimated Ni value of the tetragonal shear constant $C'=(C_{11}-C_{12})/2$ that arises from the second-moment approximation of the density of states (DOS) in TB model. For the Ni element, higher-order moments of the DOS should be accounted in future work for a more realistic value of C'.[22] However, since we are mainly concerned with the effect of concentration gradient on the lattice strain, the fact that $2C_{12}/C_{11}$ does not depend on the concentration in our model does not change the conclusions drawn in this work. In future work, more realistic calculations should however account for this property that is also often neglected in-phase field continuum models.[23]

C. Interface properties

Atomistic simulations can provide valuable information to rationalize surface and interface phenomena. In the past, the SMA potential has been quite successful in this task.[10] For instance, the complex surface reconstruction of one Ag monolayer deposited on a (111) Cu surface was elucidated.[24] More recently, the interpretation of the self-organization observed on the (111) Ag surface after the deposition of a Cu submonolayer was also possible.[25] In Sec. II A, values of the SMA parameters were determined to mimic the bulk properties of the CuNi system. In this section, we now wish to test its ability to reproduce some relaxation behaviors at the vicinity of interfaces. For this purpose, we choose the case of an ultrathin Ni film deposited on a clean (001) Cu surface which has been analyzed in detail both experimentally and theoretically.

In Fig. 2(a), we first plot the relaxed interplane distances $d_\perp(z)$ (compared to bulk Cu) calculated in a coherent 5 monolayers (ML) Ni film deposited on a Cu (001) substrate. The low-energy electron-diffraction (LEED) measurements performed by Platow *et al.*[7] on this system (from a deposition at room temperature with a rate about 0.6 ML/min followed by a brief heat treatment at 400 K) and the *ab initio* calculations from Spišák *et al.*[6] are also reported for comparison. In addition, we consider in Fig. 2(b) the situation where the Ni deposit is covered by a surfactant Cu monolayer as it was envisaged by Spišák *et al.* to interpret the LEED data. In these two limiting cases, our calculations give a tetragonal distortion of the Ni film that is similar to ones found in previous works. A tendency to slightly underesti-

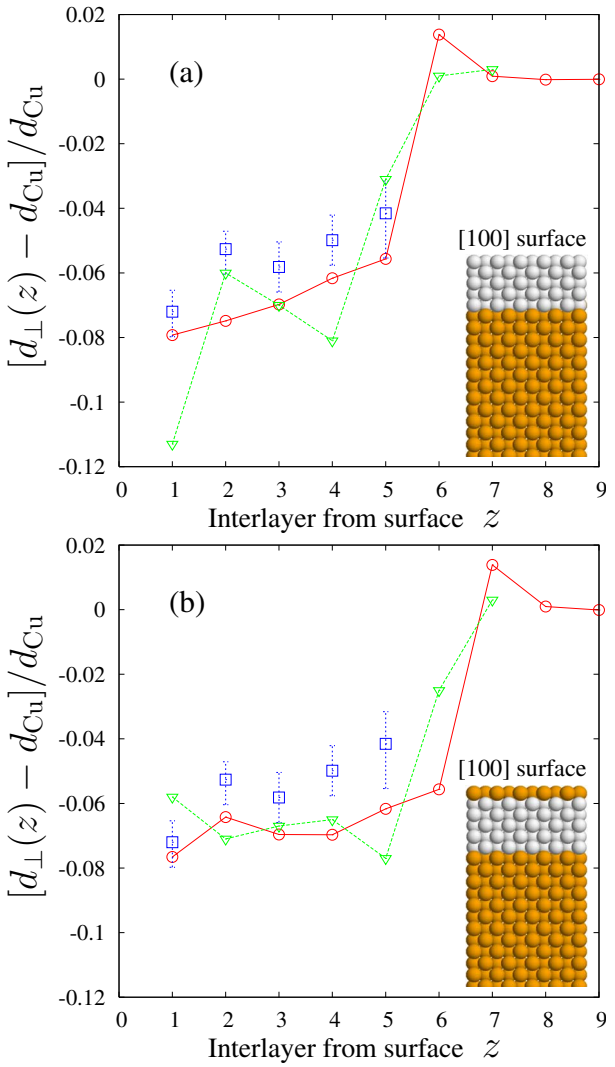

FIG. 2. (Color online) Interplane distances $d_\perp(z)$ (compared to bulk Cu, d_{Cu}) in a coherent 5 ML Ni film deposited on a Cu (001) substrate assumed without (a) and with (b) a capping Cu monolayer: (○) calculated values from the SMA potential; (□) experimental data from Ref. 7; and (▽) *ab initio* calculations from Ref. 6.

mate the Ni-Ni distances with respect to the experiment values can however be seen in our model. This is partly due to the already mentioned overestimation of the $2C_{12}/C_{11}$ ratio for the Ni element. Without any surfactant Cu layer, the interplane distances slightly increase by approaching the interface. Interestingly, this latter has an interplane distance that remains close to a Ni-Ni spacing in the distorted film. If one assumes that there is no intermixing, the calculated interfacial distance seems to slightly underestimate the experimental one. On the surface side and although the coherency strain already causes a contraction of the Ni planes, our model predicts an inward relaxation of the first surface plane in agreement with the experimental data. The capping Cu layer in our calculations mainly affects the second surface distance in an oscillatory manner that is curiously similar to the experimental one. However, it should be recalled here that according to Platow *et al.*[7] the LEED's measurements cannot give access to the composition profiles for the Cu-Ni system and therefore evidence the presence of such a capping Cu layer. Moreover, intermixing at interfaces and surfactant effects are strongly dependent on the temperature conditions, the deposition rate and on subsequent heat treatments of the film. Very recently this subject has been largely revisited by Meyerheim *et al.* (see Ref. 8) by combining both surface x-ray diffraction and molecular-dynamics simulations on that system. These authors elucidate in particular the state of intermixing in this thin film when it is deposited at low deposition rate (0.16 ML/min) and $T=300$ K. In these conditions, no surfactant effect is found and some significant intermixing occurs at the interface during the first stage of the thin-film growth.[8] More importantly for the purpose of our paper, the x-ray study of Meyerheim *et al.*[8] reveals some marked inward relaxations at the interface with a vertical Ni-Cu spacing across the intermixed interface that is close to the Ni-Ni spacing (and even shorter). This latter interfacial Cu-Ni property is rather consistent with the trends obtained from our calculations. It also indicates that usual elasticity theory will fail in predicting interplane distances near Cu/Ni interfaces as it will be shown Sec. III.

III. STRAIN IN (001) Cu/Ni MULTILAYERS

A. Sharp (001) interfaces

The case of a coherent multilayers with sharp interfaces and a free [001] surface is analyzed in this section. It is also the place where we briefly recall the continuum equations that provide the composition dependence of strain for the simple geometries considered in this work. This formalism is based on the usual linear and nonlinear elasticity theory.[26–28]

Typical multilayer considered here is made of few tens of identical Cu/Ni bilayers synthesized on a cleaved foreign substrate (for instance by magnetron sputtering on a MgO substrate). The as-grown multilayer ends with a free [001] surface. The sample is therefore free of stress in this direction z. The multilayer also remains coherent which means that the Cu and Ni regions have the same in-plane distance denoted $d_{\parallel}$ ($d_{\parallel}$ is therefore the distance between two adjacent [100] rows of atoms in the x-y planes parallel to the interfaces). When deposited on a MgO substrate, the interface coherency is generally observed for Cu/Ni multilayer having a modulation length about 40 atomic planes or less. For symmetrical bilayers, the in-plane distance is then close to the average value $d_{\parallel}=(d_{\mathrm{Cu}}+d_{\mathrm{Ni}})/2\approx 1.785$ Å.[29] In this geometry, the coherency strain causes a contraction (or a dilatation) of the interplane distances $d_{\perp}(z)$ along the z axis, if these planes contain the smallest element (nickel atoms) or the biggest element (copper atoms). For pure planes that are relatively away from the interfaces the values of the $d_{\perp}(z)$ spacings can be evaluated from the classical elasticity theory. In this framework, using Voigt notation for a cubic system with a coordinate axis taken to be the principal axis and considering that the principal stresses σ_i and strains ϵ_i obey to a state of biaxial stress we have $\sigma_1=\sigma_2=\sigma$, and $\sigma_3=\sigma_4=\sigma_5=\sigma_6=0$. This tetragonal distortion also implies that

$$\epsilon_1=\epsilon_2=\epsilon_{\parallel}=\frac{d_{\parallel}}{d_0}-1, \tag{3}$$

and

$$\epsilon_3=\epsilon_{\perp}=\frac{d_{\perp}}{d_0}-1, \tag{4}$$

where $d_0=a_0/2$ is the bulk equilibrium interplane distance. Using the linear relationship $\sigma_i=C_{ij}\epsilon_j$ between stress and strain through the elastic constant C_{ij}, one obtains

$$\epsilon_{\perp}=\frac{-2C_{12}}{C_{11}}\epsilon_{\parallel}, \tag{5}$$

and therefore a direct estimation of the resulting $d_{\perp}(z)$ interplane distances in z pure regions [denoted $d_{\perp}^{\mathrm{lin.}}(z)$ below for linear theory]. For large elastic deformations, nonlinear elasticity might be invoked. Considering the same state of biaxial stress and using a Lagrangian formulation of the principal stresses τ_i and strains η_i, we have the strain-stress relation $\tau_i=C_{ij}\eta_j+\frac{1}{2}C_{ijk}\eta_k\eta_l$ with Lagrangian strains that in our case reduce to the following nonvanishing terms:

$$\eta_1=\eta_2=\eta_{\parallel}=\epsilon_{\parallel}+\frac{1}{2}\epsilon_{\parallel}^2, \tag{6}$$

and

$$\eta_3=\eta_{\perp}=\epsilon_{\perp}+\frac{1}{2}\epsilon_{\perp}^2. \tag{7}$$

Again, the free [001] surface implies that $\tau_3=0$. Combining this condition and the strain-stress relation provides the following implicit nonlinear solution for the perpendicular strain $\eta_{\perp}$,

$$\frac{C_{111}}{2}\eta_{\perp}^2+(C_{11}+2C_{112}\eta_{\parallel})\eta_{\perp}+(C_{112}+C_{123})\eta_{\parallel}^2+2C_{12}\eta_{\parallel}=0, \tag{8}$$

and therefore the resulting $d_{\perp}(z)$ spacing in z pure regions [denoted $d_{\perp}^{\mathrm{nonlin.}}(z)$ hereafter]. Considering now an homogeneous region where along z the concentration $c(z)$ does not vary significantly, one can also use Eq. (5) [or Eq. (8) for large deformation] to estimate the interplane distance $d_{\perp}[c(z)]$ by taking into account the fact that both elastic

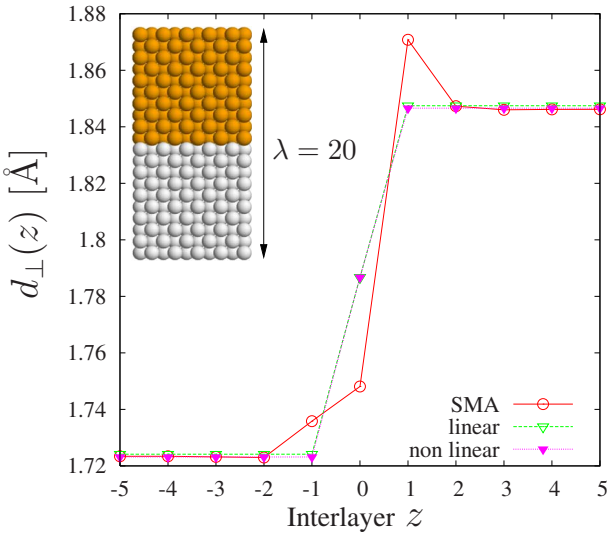

FIG. 3. (Color online) Interplane distances $d_\perp(z)$ in a coherent (001) Cu/Ni multilayer with sharp interfaces. The modulation length $\lambda=20$ planes and the in-plane distance $d_\parallel=(d_{\mathrm{Cu}}+d_{\mathrm{Ni}})/2=1.785$ Å. Calculations are obtained from (○) the SMA potential [Eq. (1)], (▼) the nonlinear continuum model [Eq. (8)], and (▽) the linear continuum model [Eq. (5)]. On the figure, spacings are reported for half a bilayer only. The Ni region (for $z<0$) and the Cu region (for $z>0$) are delimited by an Ni-Cu interplane at $z=0$.

constants and the equilibrium lattice parameter $a_0=2d_0$ of the solid solution change with c as shown in Sec. II B. Thus, according to the linear continuum approach formulated in Eq. (5) and using Eq. (2), one obtains the following local concentration dependence of the interplane distance $d_\perp^{\mathrm{lin.}}[c(z)]$:

$$d_\perp^{\mathrm{lin.}}(c) = d_\alpha(c) + d_\beta(c)\left[\sum_{n=1}^{3} \eta_n (c-c_0)^n\right] \tag{9}$$

where $d_\alpha(c)=d_0(c_0)-2C_{12}(c)/C_{11}(c)[d_\parallel-d_0(c_0)]$ and $d_\beta(c)=[1+2C_{12}(c)/C_{11}(c)]d_0(c_0)$. If, in addition, the ratio $2C_{12}(c)/C_{11}(c)$ is almost constant as obtained in Sec. II C from our SMA potential, then $d_\perp^{\mathrm{lin.}}[c(z)]$ has a simple polynomial dependence with $c(z)$.

On a discrete lattice where concentration $c(i)$ are defined per plane i, the spacing between two adjacent planes i and $i+1$ is evaluated from Eq. (9) by replacing $c(z)$ by the average value $[c(i)+c(i+1)]/2$. Similarly from Eq. (8), the concentration dependence of C_{ij}, C_{ijk}, and d_0 gives an estimation of $d_\perp^{\mathrm{nonlin.}}[c(z)]$ in presence of large deformation. In order to have a direct quantitative comparison between atomistic and continuum calculations of the strain field, values of the lattice parameter and of the elastic constants are the ones given by the SMA potential in Sec. II B. In particular for $d_\perp^{\mathrm{lin.}}(c)$, the term $2C_{12}(c)/C_{11}(c)$ is fixed to a constant value of 1.49. For $d_\perp^{\mathrm{nonlin.}}(c)$, elastic constants are also taken from Table II and are chosen to vary linearly with c.

In Fig. 3, we first consider the case of a coherent symmetrical (001) Cu/Ni multilayer with perfectly sharp interfaces. The modulation length λ of a bilayer is fixed to 20 planes and the in-plane distance $d_\parallel=(d_{\mathrm{Cu}}+d_{\mathrm{Ni}})/2=1.785$ Å. Molecular statics calculations, within the SMA potential described in Sec. II, are performed on a bilayer having periodic conditions in the three directions. By varying the size of the simulation box along the z axis, one obtains a minimum of the total energy of the system that corresponds to the relaxed structure that is free of stress along the z direction. The resulting $d_\perp^{\mathrm{SMA}}(z)$ profile is plotted in Fig. 3 and compared to $d_\perp^{\mathrm{lin.}}(z)$ and $d_\perp^{\mathrm{nonlin.}}(z)$. Far from the interfaces, the interplane distances predicted from the three approaches are very close. The gain in using nonlinear theory from Eq. (8) can be noticed, this remains however a small refinement with respect to the linear model of Eq. (9) due to the low $\epsilon_\perp$ values reached (about 2%). Considering now the strain at the interfaces, atomistic calculations reveal a marked interfacial relaxation that spreads over five planes. The $d_\perp^{\mathrm{SMA}}(z)$ profile is asymmetric with a Ni-Cu interplane distance that is close to the one found in the Ni region. This behavior is similar to the situation observed at the interface of the 5 ML Ni/Cu film shown in Fig. 2. Moreover in Fig. 3, the interfacial values of $d_\perp^{\mathrm{lin.}}$ and $d_\perp^{\mathrm{nonlin.}}$ are also reported. Clearly, applying the continuum models to determine the interfacial distance is not correct since by definition the concentration profile varies strongly in this region. It is however instructive to show that a brute application of these models near interfaces fails in describing the strain field. In Secs. III B and III C, a systematic study of Cu/Ni multilayers with diffuse interfaces will enable us to identify the main terms that are missing in the continuum models.

B. Diffuse (001) interfaces

Classical continuum models that link composition and strain fields together cannot be applied in multilayer regions where the composition varies strongly. This has been shown in Sec. III A for the ideal case of a multilayer having perfectly sharp interfaces. For diffuse interfaces, what is the typical wavelength above which elasticity theories become valid? To answer this point we have performed systematic MS calculations on multilayers presenting sinusoidal concentration profiles along the z direction and with different wavelengths λ. As in Sec. III A, we consider the same state of biaxial stress and use the same relaxation procedure to determine the strain established in the coherent multilayer. The Ni and Cu atoms are now randomly distributed per plane i, according to the concentration profile,

$$c(i) - c_0 = c_0 \cos(2\pi i/\lambda), \tag{10}$$

with $c_0=0.5$. Again, the fully relaxed positions of the atoms in these bilayers are obtained for a stress null along z and a constant in-plane distance $d_\parallel=(d_{\mathrm{Cu}}+d_{\mathrm{Ni}})/2=1.785$ Å. The position of a given plane is calculated by averaging the positions of the atoms that belong to this plane. These calculations are made for simulation boxes containing at least 400 atoms/plane to ensure low uncertainty on the average plane positions.

In Fig. 4, we report the interplane distance profiles $d_\perp^{\mathrm{SMA}}(z)$ for sinusoidal concentration profiles of wavelengths $\lambda=10$, 20, and 30 planes. The atomistic calculations are compared to the $d_\perp^{\mathrm{lin.}}(z)$ and $d_\perp^{\mathrm{nonlin.}}(z)$ profiles predicted by the

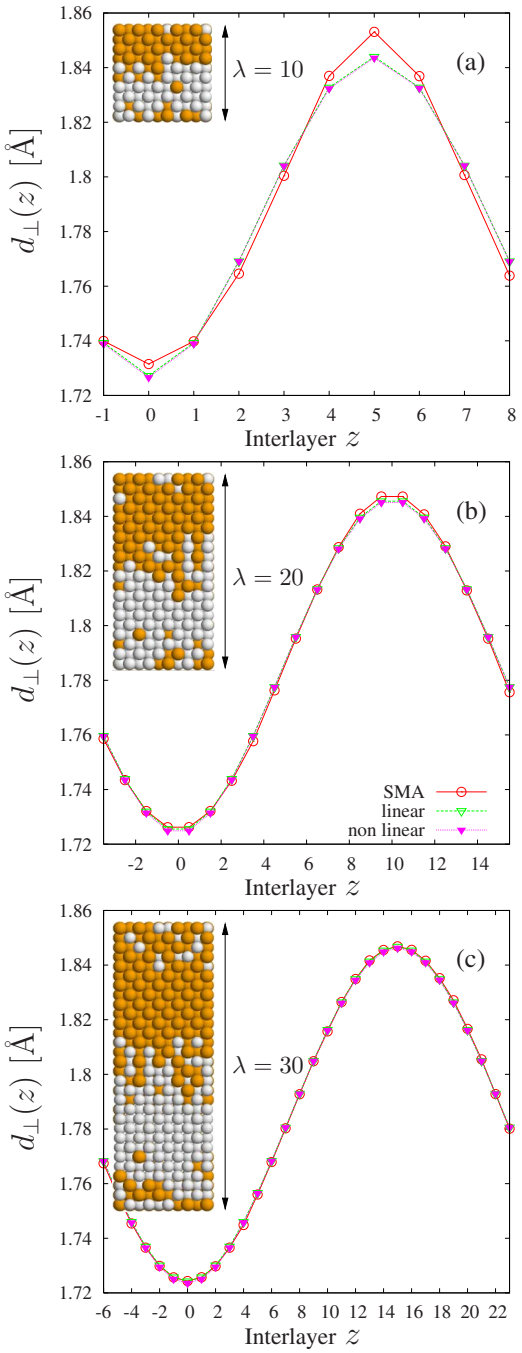

FIG. 4. (Color online) $d_\perp(z)$ profiles obtained from (001) Cu/Ni multilayers having sinusoidal composition of wavelength λ, from (○) the SMA potential [Eq. (1)], (▼) the nonlinear [Eq. (8)], and (▽) the linear continuum models [Eq. (5)]. For $z=0$, the Ni concentration is maximum.

linear [Eq. (9)] and the nonlinear [Eq. (8)] continuum models for these bilayers. For the large composition wavelength (λ =30 planes) considered in Fig. 3(c), both atomistic and continuum descriptions converge to very close $d_\perp(z)$ curves. For a sinusoidal composition field, one obtains an almost pure sinusoidal distance profile of the same wavelength. From the linear model of Eq. (9), this result becomes obvious if one bears in mind that the term $2C_{12}(c)/C_{11}(c)$ is taken as constant and $\eta_1 \gg \eta_2, \eta_3$ for the CuNi system. Note that this simple linear relation between $d_\perp(z)$ and $c(z)$ can be already found in the very first studies on the x-ray characterizations of multilayer systems.[2] For λ=20 planes in Fig. 3(b), only slight differences might be noticed and the use of continuum models remains quite accurate. It is for shorter composition wavelengths (below λ=20) that deviations appear on the strain-composition relationships given by the two approaches. From Fig. 3(a) where the case λ=10 is reported, one can note that the average value of $d_\perp^{\mathrm{SMA}}(z)$ profile is slightly increased and its amplitude decreased with respect to the ones given by elasticity theories. More significantly for short λ, atomistic calculations reveal that the strain response to a sinusoidal composition profile is not simply a sinusoid with the same wavelength but rather some additional harmonics appear in the lattice spacing profile.

C. Composition/strain model

To quantify the deviations from continuum models observed in our atomistic calculations for short composition wavelength, we perform a Fourier analysis of the interplane distance profiles. For this purpose the various $d_\perp(z)$ profiles obtained in Sec. III B from diffuse sinusoidal multilayers are now formulated according to the following Fourier series:

$$d_\perp(z) = \sum_n a_n(\lambda)\cos(nZ), \tag{11}$$

where $Z=2\pi z/\lambda$ and $a_n(\lambda)$ are the Fourier coefficients to be adjusted for a given wavelength λ. Note that the $a_n(\lambda)$ coefficients can be also derived analytically in the framework of the linear model of Eq. (9). Indeed, considering the $c(i)$ expression given by Eq. (10) and again a constant ratio for the $2C_{12}(c)/C_{11}(c)$ term in Eq. (9), one obtains

$$d_\perp^{\mathrm{lin.}}(z) = d_\alpha + d_\beta\left[\sum_{n=1}^{3} \eta_n\gamma_n \cos^n(Z)\right] \tag{12a}$$

$$= \sum_{n=0}^{3} a_n^{\mathrm{lin.}}(\lambda)\cos(nZ), \tag{12b}$$

with $\gamma_n=[c_0\cos(\pi/\lambda)]^n$ and the following Fourier coefficients: $a_0^{\mathrm{lin.}}(\lambda)=d_\alpha+d_\beta\eta_2\gamma_2/2$, $a_1^{\mathrm{lin.}}(\lambda)=d_\beta(\eta_1\gamma_1+3\eta_3\gamma_3/4)$, $a_2^{\mathrm{lin.}}(\lambda)=d_\beta\eta_2\gamma_2/2$, and $a_3^{\mathrm{lin.}}(\lambda)=d_\beta\eta_3\gamma_3/4$. Thus, even for the linear model, some λ dependence of the $a_n^{\mathrm{lin.}}$ coefficients is expected due the discretization of the composition profile on the crystal lattice (i.e., the approximation that $c(z)=[c(i)+c(i+1)]/2$). We will verify however that the influence of λ on the $a_n^{\mathrm{lin.}}$ is small in agreement with the previous observations that $d_\perp(z)$ remains close to a sinusoid within this model.

For composition wavelengths λ ranging from 10 to 40 planes, we report in Fig. 5 the $a_n(\lambda)$ coefficients resulting from the $d_\perp^{\mathrm{lin.}}(z)$, the $d_\perp^{\mathrm{nonlin.}}(z)$ and the $d_\perp^{\mathrm{SMA}}(z)$ profiles. The coefficient $a_3(\lambda)$ is negligible here and not shown.

Considering first the two analytical approaches in Fig. 5, we note that the $a_n^{\mathrm{nonlin.}}(\lambda)$ given by the nonlinear model [Eq. (8)] have variations similar to the $a_n^{\mathrm{lin.}}$ ones. Numerically, each $a_n^{\mathrm{nonlin.}}(\lambda)$ and $a_n^{\mathrm{lin.}}$ terms differ mainly by a constant and

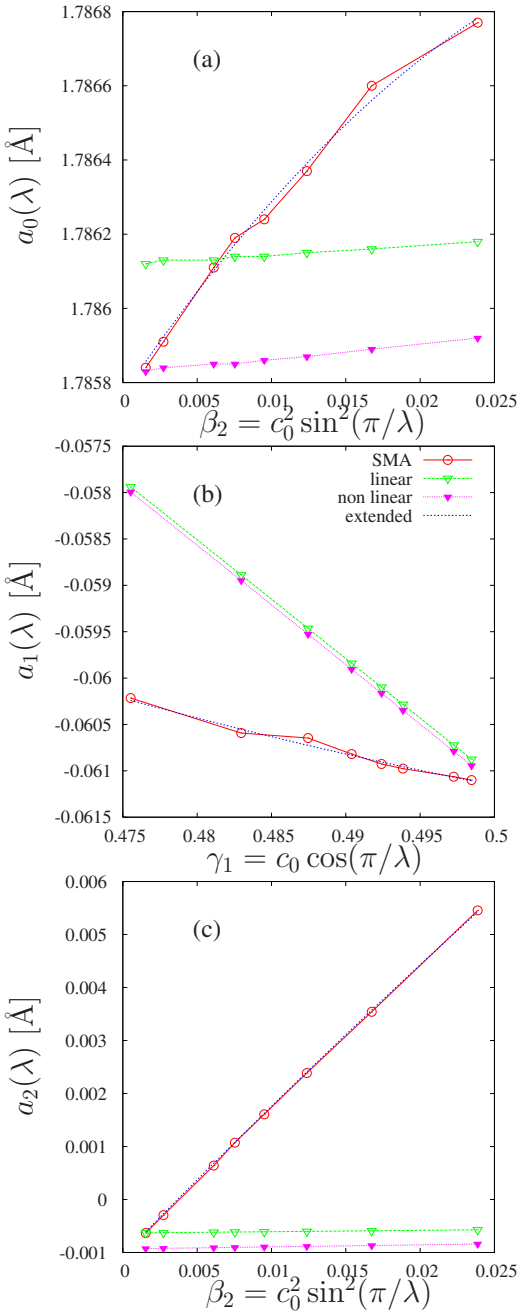

FIG. 5. (Color online) Fourier components $a_n(\lambda)$ of the $d_\perp(z)$ profiles obtained in Fig. 4. On the x axis, λ varies from 10 to 40 planes through the terms β_2 in (a),(c), and γ_1 in (b). The Fourier coefficients are calculated from the different approaches (see text): (○) a_n^{SMA}, (▼) $a_n^{\mathrm{nonlin.}}$, (▽) $a_n^{\mathrm{lin.}}$, and (dotted line) $a_n^{\mathrm{ext.}}$ from Eq. (18).

can be related together through the following equation:

$$a_n^{\mathrm{nonlin.}}(\lambda) \approx a_n^{\mathrm{lin.}}(\lambda) + k_n \tag{13}$$

where k_n are constants.

Comparing now the $a_n^{\mathrm{nonlin.}}(\lambda)$ to the $a_n^{\mathrm{SMA}}(\lambda)$ resulting from the molecular statics calculations, we note that they both converge to close values when λ becomes large [i.e., when $\beta_2 = c_0^2 \sin^2(\pi/\lambda)$ tends to zero in Figs. 5(a) and 5(c) and $\gamma_1 = c_0 \cos(\pi/\lambda)$ tends to 0.5 in Fig. 5(b)]. The main result to be underlined in Fig. 5 is certainly the specific λ dependence of the $a_n^{\mathrm{SMA}}(\lambda)$. Whereas the variations in $a_0^{\mathrm{SMA}}(\lambda)$ and $a_1^{\mathrm{SMA}}(\lambda)$ remain low, the $a_2^{\mathrm{SMA}}(\lambda)$ coefficient strongly increases when λ decreases.

These observations suggest that some terms are missing in the continuum models to capture the strain profiles given by the atomistic calculations at short wavelength. Seeking for an extended continuum model, one can first exclude some additional c^n terms since the nonlinear elastic model gives the correct Fourier coefficients for large λ. New terms depending on the concentration gradient ∇c are therefore to be considered in details. Since the $d_\perp(z)$ spacing does not depend on the sign of ∇c, additional terms should obey to this symmetry property. Thus, the difference between $d_\perp^{\mathrm{SMA}}(c)$ and $d_\perp^{\mathrm{nonlin.}}(c)$ might take the general form,

$$d_\perp^{\mathrm{SMA}}(c) = d_\perp^{\mathrm{nonlin.}}(c) \tag{14a}$$

$$+ f[(\nabla c)^{2n}, (\nabla^{2n} c)^k, c^k (\nabla c)^{2n}, c^k \nabla^{2n} c, \ldots], \tag{14b}$$

where n and k are integers and f is a linear function to be determined. Hopefully, using Eqs. (12a), (12b), (13), (14a), and (14b), it is possible to identify the leading terms in the expansion of f that reproduce well the λ dependence of the a_n^{SMA} coefficients in Fig. 5. Indeed, using Eq. (10) and expressing via finite differences the Laplacian $\nabla^2 c$ for the distance $d_\perp(z)$ between the planes i and $i+1$, one writes $\nabla^2 c \propto [c(i+2) - c(i+1)] - [c(i) - c(i-1)]$ and obtains

$$\nabla^2 c \approx 4(\gamma_3/c_0^2 - \gamma_1)\cos(Z)/d_0^2. \tag{15}$$

This term directly controls the a_1 component in Fig. 5(b) and enables to mimic the linear decrease with γ_1 observed in a_1^{SMA}. On the other hand, the combination of a term $(\nabla c)^2$ and a crossed term $(c - c_0)\nabla^2 c$ will cause a change of both the $a_0(\lambda)$ and $a_2(\lambda)$ Fourier coefficients in the following manner:

$$(\nabla c)^2 \approx 2\beta_2[1 - \cos(2Z)]/d_0^2, \tag{16}$$

and

$$(c - c_0)\nabla^2 c \approx 2(\beta_2^2/c_0^2 - \beta_2)[1 + \cos(2Z)]/d_0^2, \tag{17}$$

with the finite difference approximation $\nabla c \propto c(i+1) - c(i)$. A linear combination of $(\nabla c)^2$ and $(c - c_0)\nabla^2 c$ allows a very fine description of the β_2 dependence of the atomistic calculations as it is shown in Figs. 5(a) and 5(c).

To summarize, we establish an extended composition/strain relation (denoted $d_\perp^{\mathrm{ext.}}(c)$) in presence of strong concentration gradients that writes

$$d_\perp^{\mathrm{SMA}}(c) \approx d_\perp^{\mathrm{ext.}}(c), \tag{18a}$$

$$= d_\perp^{\mathrm{nonlin.}}(c) + \kappa_0(\nabla c)^2 + [\kappa_1 + \kappa_2(c - c_0)]\nabla^2 c, \tag{18b}$$

where $\kappa_0 = -0.182$ Å^3, $\kappa_1 = 0.039$ Å^3, and $\kappa_2 = -0.544$ Å^3, and $d_0 = 1.786$ Å for the CuNi system.

IV. DISCUSSION

We have mentioned in Sec. I that a reliable composition/strain model would be valuable to interpret precisely x-ray

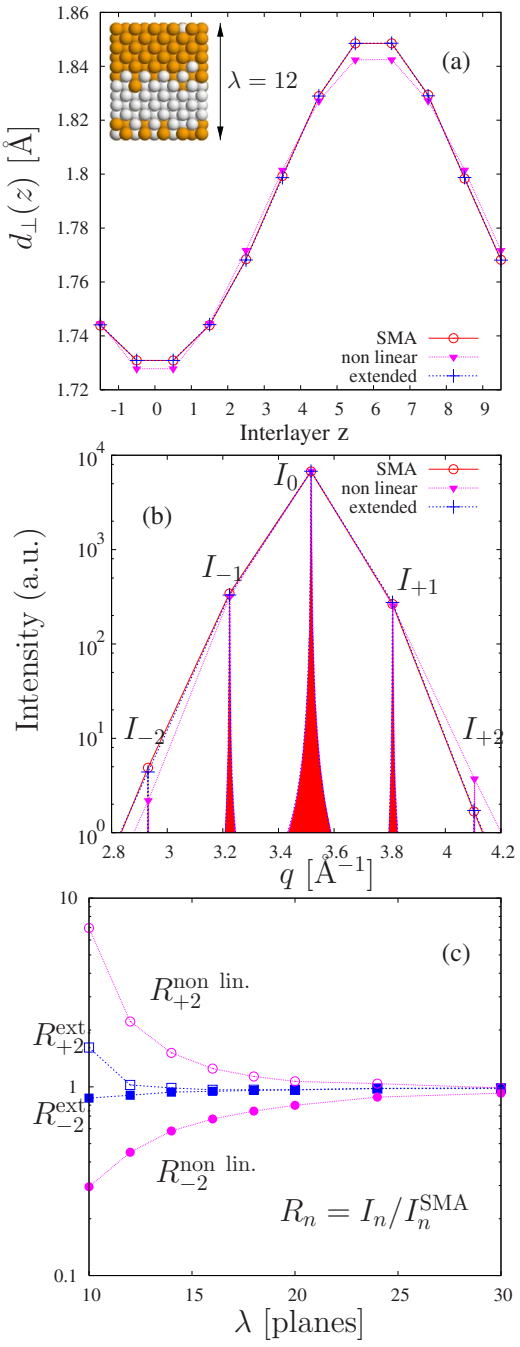

FIG. 6. (Color online) From a sinusoidal ($\lambda=12$, $N=100$) Cu/Ni multilayer, we report in (a) $d_{\perp}^{\mathrm{SMA}}(z)$ (○) from Eq. (1), $d_{\perp}^{\mathrm{nonlin.}}(z)$ (▼) from Eq. (8), and $d_{\perp}^{\mathrm{ext.}}(z)$ (+) from Eq. (18). In (b), the corresponding x-ray spectra [Eq. (19)] are shown with the positions of the main satellite peaks. In (c), intensity ratios of the second-order satellite peaks versus λ for $N=100$.

scattering spectra of multilayers. In reverse, it is also of interest to quantify if such experimental techniques would be able to evidence the composition gradient effects established in this work [in Eq. (18)] for the CuNi system. To illustrate this point, we first show in Fig. 6(a) for a sinusoidal composition profile with $\lambda=12$ planes, the interplanar spacings given by the nonlinear continuum model [$d_{\perp}^{\mathrm{nonlin.}}(z)$ from Eq. (8)], our extended model [$d_{\perp}^{\mathrm{ext.}}(z)$ from Eq. (18)] and the $d_{\perp}^{\mathrm{SMA}}(z)$ profiles of the atomistic calculations. Clearly in Fig. 6(a), the extended model derived in this work enables to capture the composition gradient effects since $d_{\perp}^{\mathrm{ext.}}(z)$ and $d_{\perp}^{\mathrm{SMA}}(z)$ are almost superposed and differ from the $d_{\perp}^{\mathrm{nonlin.}}(z)$ profile. In order to evaluate if such differences are measurable from x-ray diffraction, we then report in Fig. 6(b) the out-of-plane x-ray spectra resulting from such sinusoidal multilayers with a number of bilayers that is arbitrarily fixed to $N=100$. Calculations are made in the framework of the kinematic theory of x-ray diffraction in the simple Bragg geometry where the scattering vector $\mathbf{q}$ is parallel to the z direction. From the relaxed z positions z_j of the Ni and Cu atoms obtained in our atomistic calculations in one periodic bilayer, the x-ray scattered intensity $I(q)$ of one multilayer containing N identical bilayers can be evaluated from the following product:[2]

$$I(q) \propto |S(q)|^2 |F(q)|^2, \tag{19}$$

where

$$S(q) = \frac{\sin(Nq\lambda\bar{d}/2)}{\sin(q\lambda\bar{d}/2)} \tag{20}$$

is the interference function of the superlattice with $\bar{d}$ defined as the average interplane distance and $F(q)$ is the structure factor of the bilayer that is calculated by summing over all the j atoms

$$F(q) = \sum_j f_j \exp(-iqz_j), \tag{21}$$

with f_j being the atomic scattering factor of the jth atom. From Refs. 30 and 31, at the x-ray energy corresponding to the copper emission line K_{α}, we use $f_j=f_{\mathrm{Ni}}=15+i0.51$ for a Ni atom and $f_j=f_{\mathrm{Cu}}=17+i0.59$ for a Cu one. On the other hand, from the continuum composition/strain models described in this work, a direct calculation of the structure factor $F(q)$ is also possible for a given concentration profile. The sum in Eq. (21) is made over all the i planes with a scattering factor per plane $f_i=f_{\mathrm{Ni}}c(i)+f_{\mathrm{Cu}}[1-c(i)]$. The position z_i of the i plane is directly deduced from the corresponding $d_{\perp}(z)$ profile.

In Fig. 6(b), the comparison of the main satellite peaks of the calculated x-ray spectra indicates that some signature of the concentration gradients effects should be found in the intensities of the second-order peaks I_{+2} and I_{-2}. The strength of the I_{+2} peak is overestimated (and I_{-2} is underestimated) by about a factor 2 if one neglects gradient effects in a $\lambda=12$ multilayer. In other words, composition gradients have an asymmetrical effect on the $I_{\pm2}$ satellites. To confirm this trend for other composition wavelengths, we plot in Fig. 6(c) the intensity ratios $R_{\pm2}^{\mathrm{nonlin.}}=I_{\pm2}^{\mathrm{nonlin.}}/I_{\pm2}^{\mathrm{SMA}}$ and $R_{\pm2}^{\mathrm{ext.}}=I_{\pm2}^{\mathrm{ext.}}/I_{\pm2}^{\mathrm{SMA}}$ as a function of λ. One can observe that indeed, $R_{\pm2}^{\mathrm{nonlin.}}$ increase or decrease with λ while the ratios $R_{\pm2}^{\mathrm{ext.}}$ remain close to one when the composition gradient terms are accounted for through the extended model in Eq. (18).

V. CONCLUSION

In this work, we investigate the relationship between strain and composition in coherent Cu-Ni multilayers. The initial motivation was to improve the interpretation of x-ray diffraction experiments by testing if the continuum models generally used for this purpose could be safely applied on these objects where the composition varies on the nanoscale. Along this study, we faced an important property of these metallic systems that render unsuitable the use of the classical models: the presence of interfacial relaxations and composition gradient effects. These observations were made from atomistic calculations of the strain fields within tight-binding potentials. A systematic exploration of strain in (100) sinusoidal multilayers is then developed. This Fourier analysis allows us to derive an extended continuum model that accounts for the composition gradient effects on the coherency strain [Eq. (18)]. Interestingly, the additional terms that are necessary to bridge the gap between the classical description and atomistic calculations should be significant enough to change the shape of x-ray spectra as it is discussed in this paper. X-ray diffraction experiments are currently performed to verify this property. From a theoretical viewpoint, this work leaves open questions that should be addressed in future work: (i) from our extended model in Eq. (18), the dependence of coefficient κ_i with the in-plane distance $d_{\|}$ has to be studied to investigate other strain constrains (for instance in coherent deposited films). (ii) The formulation given in Eq. (18) offers an interesting basis to derive a complementary expression of the elastic energy term in Cahn's model[3] that would account for the effect of composition gradients on strain.

ACKNOWLEDGMENT

We wish to thank M. Gailhanou for useful discussions.

*Corresponding author; jean-marc.roussel@univ-cezanne.fr

[1] J.-M. Roussel and P. Bellon, Phys. Rev. B **73**, 085403 (2006).
[2] A. Guinier, *X-Ray Diffraction: Crystals, Imperfect Crystals, and Amorphous Bodies* (Dover, New York, 1994).
[3] J. W. Cahn, Acta Metall. **9**, 795 (1961).
[4] V. Rosato, M. Guillopé, and B. Legrand, Philos. Mag. A **59**, 321 (1989).
[5] F. Ducastelle, *Order and Phase Stability in Alloys* (North-Holland, Amsterdam, 1991).
[6] D. Spisák and J. Hafner, J. Phys.: Condens. Matter **12**, L139 (2000).
[7] W. Platow, U. Bovensiepen, P. Poulopoulos, M. Farle, K. Baberschke, L. Hammer, S. Walter, S. Müller, and K. Heinz, Phys. Rev. B **59**, 12641 (1999).
[8] H. L. Meyerheim, D. Sander, N. N. Negulyaev, V. S. Stepanyuk, R. Popescu, I. Popa, and J. Kirschner, Phys. Rev. Lett. **100**, 146101 (2008).
[9] F. Ducastelle, J. Phys. (Paris) **31**, 1055 (1970).
[10] G. Tréglia and B. Legrand, in *Tight-Binding Approach to Computational Materials Science*, edited by P. E. A. Turchi, A. Gunis, and L. Colombo, MRS Symposia Proceedings No. 491 (Materials Research Society, Pittsburgh, 1998), p. 275.
[11] J. Creuze, F. Berthier, R. Tétot, and B. Legrand, Phys. Rev. B **62**, 2813 (2000).
[12] J. H. Rose, J. R. Smith, F. Guinea, and J. Ferrante, Phys. Rev. B **29**, 2963 (1984).
[13] R. Hultgren, P. D. Desai, D. T. Hawkins, M. Gleiser, and K. K. Kelley, *Selected Values of the Thermodynamic Properties of Binary Alloys* (American Society for Metals, Metals Park, OH, 1973).
[14] S. G. Epstein and O. N. Carlson, Acta Metall. **13**, 487 (1965).
[15] B. R. Coles, J. Inst. Met. **84**, 346 (1956).
[16] F. Lihl, H. Ebel, A. Reichl, and A. Kaminitschek, Z. Metallkd. **59**, 735 (1968).
[17] A. K. Jena, D. Gulati, and T. R. Ramachandran, Z. Metallkd. **72**, 847 (1981).
[18] T. Suzuki, A. V. Granato, and J. F. Thomas, Phys. Rev. **175**, 766 (1968).
[19] J. F. Thomas, Phys. Rev. B **7**, 2385 (1973).
[20] Y. Hiki and A. V. Granato, Phys. Rev. **144**, 411 (1966).
[21] V. P. N. Sarma and P. J. Reddy, Philos. Mag. **27**, 769 (1973).
[22] M. Nastar and F. Willaime, Phys. Rev. B **51**, 6896 (1995).
[23] A. Khachaturyan, *Theory of Structural Transformations in Solids* (Wiley, New York, 1983).
[24] I. Meunier, G. Tréglia, J.-M. Gay, B. Aufray, and B. Legrand, Phys. Rev. B **59**, 10910 (1999).
[25] F. Bocquet, C. Maurel, J.-M. Roussel, M. Abel, M. Koudia, and L. Porte, Phys. Rev. B **71**, 075405 (2005).
[26] C. Teodosiu, *Elastic Models of Crystal Defects* (Springer-Verlag, Berlin, 1982).
[27] J. Weaver, J. Phys. Chem. Solids **37**, 711 (1976).
[28] G. Abadias, A. Marty, and B. Gilles, Acta Mater. **46**, 6403 (1998).
[29] F. Gao, M.-C. Benoudia, J.-M. Roussel, S. Labat, O. Thomas, D. L. Beke, G. Langer, and M. K. Varga (unpublished).
[30] S. Brennan and P. Cowan, Rev. Sci. Instrum. **63**, 850 (1992).
[31] P. J. Brown, A. G. Fox, E. N. Maslen, M. A. O'Keefe, and B. T. M. Willis, *International Tables for Crystallography* (Kluwer Academic Publishers, Dordrecht, 1999), Vol. C, p. 551.